Magnetism in the spin-density-wave alloy $Cr_{1-x}Mn_x$ ($x=0.007$)

B. J. Sternlieb, E. Lorenzo, and G. Shirane
Department of Physics, Brookhaven National Laboratory, Upton, New York 11973

S. A. Werner
Physics Department, University of Missouri, Columbia, Missouri, 65211

E. Fawcett
Physics Department, University of Toronto, Toronto, Canada M5S 1A7

(Received 3 June 1994)

Neutron-scattering measurements characterizing the magnetic behavior of single-crystal $Cr_{1-x}Mn_x$ ($x=0.007$) are reported. Four distinct phases are observed: paramagnetic, commensurate spin density wave (SDW), transversely polarized incommensurate SDW, and longitudinally polarized incommensurate SDW. Transitions between these phases occur at $T_N=455$ K, $T_{IC}=182$ K, and $T_{SF}=85$ K, respectively. A revised phase diagram for the $Cr_{1-x}Mn_x$ alloy system is presented in light of these data.

INTRODUCTION

The rich antiferromagnetic behavior of chromium and its alloys has attracted a great deal of interest in recent years.[1,2] The $[Ar]3d^54s^1$ electronic configuration and bcc crystal structure of pure chromium metal result in a band structure whose major components in reciprocal space are an electron octahedron $\mathcal{S}_e$ at the zone center Γ and a somewhat larger hole octahedra $\mathcal{S}_h$ located at the $\{100\}$ corners H of the Brillouin zone. Though the size mismatch between these octahedra prohibits the commensurate mapping of $\mathcal{S}_e$ onto $\mathcal{S}_h$, large portions of these surfaces can be "nested" via the incommensurate vectors $\mathbf{Q}_+=(1+\delta,0,0)$ or $\mathbf{Q}_-=(1-\delta,0,0)$ as shown in Fig. 1(a). This nesting, in combination with the Coulomb attraction between electrons and holes, results in a weakly first-order[3,4] transition to an incommensurate, transversely polarized spin-density-wave (TSDW) phase below the Néel temperature $T_N=311$ K. A second first-order transition, to a longitudinally polarized spin-density-wave (LSDW) phase, occurs at the spin-flip temperature $T_{SF}=121$ K.

The addition of electrons to pure chromium, by alloying with either manganese or rhenium, increases the size of $\mathcal{S}_e$ relative to $\mathcal{S}_h$. For dilute $Cr_{1-x}Mn_x$ alloys with compositions x below the triple point concentration, $x_{tr}\approx 0.3\%$, this improved nesting results in an increase in the Néel temperature and a reduction in the magnitude of the incommensurate offset, δ. The character of the magnetic phase transition changes dramatically at higher Mn concentrations; as $x>x_{tr}$, the incommensurate parameter δ falls discontinuously to zero as shown in Fig. 1(b) and the SDW phase observed below T_N is commensurate with the crystal lattice.[5] Although the free energy in this doping regime favors a commensurate transition, $\mathcal{S}_e$ remains smaller than $\mathcal{S}_h$, and at lower temperatures, if x is less than $\sim 1.4\%$, a first-order and strongly hysteretic transition occurs at the commensurate-incommensurate

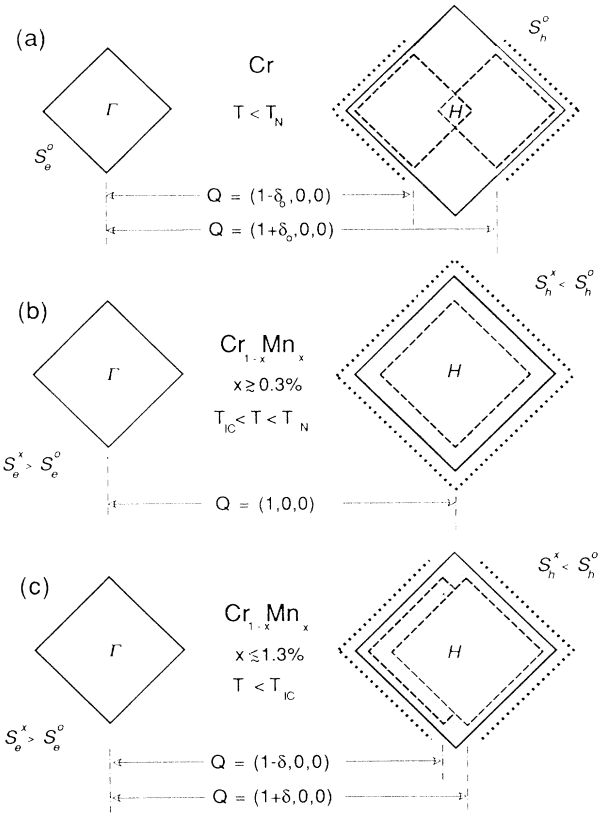

FIG. 1. Nesting of electron Γ and hole H Fermi surface octahedra in (a) pure Cr and (b), (c) $Cr_{1-x}Mn_x$. The dissimilar size of these two surfaces in pure Cr results in nesting that is incommensurate at all temperatures below T_N. In $Cr_{1-x}Mn_x$, for $x\gtrsim 0.3\%$, the nesting vector, and consequently the resulting spin-density-wave phase, are commensurate (b) with the crystal lattice below the Néel transition T_N. At lower temperatures, provided $x\lesssim 1.3\%$, the free energy of $Cr_{1-x}Mn_x$ favors a transition to incommensurate nesting (c).

(IC) transition temperature T_{IC} to an incommensurate phase as shown in Fig. 1(c).[6] At higher Mn concentrations, the free energy associated with the commensurate phase is less than the incommensurate free energy at all temperatures and no commensurate-incommensurate phase transition is observed.

The magnetic dynamics of $Cr_{1-x}Mn_x$ alloys have yet to be studied in detail. Efforts are currently underway to (1) study the impact of electron (Mn) doping on the unusual energy and polarization dependence of the magnetic excitations observed in the ground state of pure chromium,[7,8] (2) investigate the role magnetic dynamics play in the commensurate-incommensurate transition, and (3) compare the paramagnetic dynamics of $Cr_{1-x}Mn_x$ alloys with the results of Noakes *et al.*[9] in pure Cr and the hole-doped alloy system $Cr_{1-x}V_x$.

These questions are complicated, below T_N, by the body-centered-cubic symmetry of chromium and its alloys, which results in the formation of three distinct **Q** domains, shown in Fig. 2(a). Scattering from the six incommensurate magnetic satellites associated with these **Q** domains is difficult to resolve, since the separation between satellites is comparable to normal spectrometer momentum resolutions.[10] In pure chromium, a single-domain or single-**Q** sample, with elastic magnetic peaks at $\mathbf{Q}_{\pm}=(1\pm\delta,0,0)$, can be produced by cooling through T_N with a sufficiently strong magnetic field applied along the [100] crystal axis as shown in Fig. 2(b).[3] This single-**Q** preparation greatly simplifies both the acquisition and analysis of neutron-scattering data. However, so far, very little information exists on the applicability of field cooling to Cr alloys,[11] particularly those with commensurate transitions.

An additional source of confusion in the study of $Cr_{1-x}Mn_x$ is the difficulty associated with homogeneous sample preparation. In particular, some uncertainty exists in the literature, as may be seen in the magnetic phase diagram given in the review by Fawcett *et al.*,[2] regarding the phase boundaries separating the paramagnetic, commensurate SDW, and incommensurate TSDW and LSDW phases at Mn concentrations beyond the tricritical point.

Following a brief experimental description, we present elastic scattering measurements characterizing a large single $Cr_{1-x}Mn_x$ ($x=0.007$) crystal to be used in future inelastic work. These data are used to construct a revised magnetic phase diagram for this system. Attempts to produce a single-**Q** sample both by field cooling through the paramagnetic-commensurate transition at T_N and by field cooling through the commensurate-incommensurate temperature T_{IC} are also discussed.

EXPERIMENTAL CONDITIONS

The $Cr_{1-x}Mn_x$ crystal used in these measurements, referred to below as CrMn#1, was grown by an arc zone method at the Materials Preparation Center of Ames Laboratory. An initial Mn concentration of $x=0.73\%$ was used in the melt. The Mn concentration of the finished crystal was determined by means of standard x-ray fluorescence techniques. The measured concentration $x=0.7\%$ was found to be fairly uniform over the entire surface of the sample. This reduction from the "as-grown" Mn concentration can be attributed to high Mn vapor pressures present during crystal growth. The sample has a 1.0° full width at half maximum (FWHM) mosaic and dimensions $\sim 1\times 1\times 4$ cm^3.

The measurements were performed on the H4M triple-axis spectrometer at Brookhaven National Laboratory's High Flux Beam Reactor. The (002) reflection of pyrolytic graphite was used to monochromate and analyze the incident and scattered neutrons. A pyrolytic graphite filter was used to remove higher-order (λ/n) contamination from the scattered beam. All measurements were done using a 40′-40′-*S*-40′-40′ collimation configuration and unpolarized neutrons with a fixed final energy of $E_f=14.7$ meV.

Prior to the measurements presented below, the sample

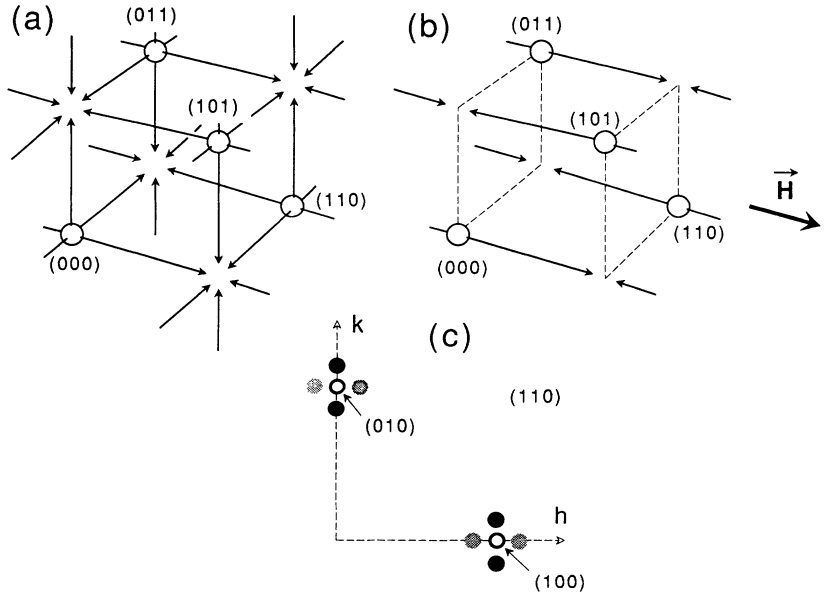

FIG. 2. Reciprocal space showing magnetic (arrow heads) and nuclear (circles) Bragg reflections in (a) polydomain- and (b) single-**Q** Cr. The gray and black circles shown in the ($hk0$) scattering plane (c) indicate the two distinct **Q** domains in an incommensurate, polydomain sample accessible in this scattering geometry. Finite spectrometer resolutions allow the satellites above and below the plane to contribute to the observed scattering intensity at the commensurate positions (open circles).

was field cooled from paramagnetic temperatures $T > 500$ K into the commensurate SDW phase at room temperature with a 14-T field applied along the $(h00)$ axis. The sample was then remounted in a closed-cycle He refrigerator with the $(00l)$ axis normal to the scattering plane to allow the study of momentum transfers $\kappa \in (hk0)$. Additional measurements, to test the feasibility of producing a single-Q phase by field cooling through the IC transition, were made using a flow cryostat with an integral superconducting magnet capable of applying a 6-T field normal to the $(hk0)$ scattering plane.

ELASTIC RESULTS

Generally, the dependence of the elastic magnetic neutron-scattering cross section,[12]

$$\left[\frac{d\sigma}{d\Omega}\right]_{\rm el} \sim |\hat{\mathbf{k}} \times \{\mathcal{M}(\boldsymbol{\kappa}) \times \hat{\boldsymbol{\kappa}}\}|^2 ,$$

on the Fourier transform of the magnetization,

$$\mathcal{M}(\mathbf{k}) = \int \langle \mathbf{M}(\mathbf{r}) \rangle e^{i\mathbf{k}\cdot\mathbf{r}} d\mathbf{r} ,$$

allows only magnetic moments normal to the neutron momentum transfer $\boldsymbol{\kappa} \equiv \mathbf{k}_i - \mathbf{k}_f$ to contribute to the measured scattering intensity. In the incommensurate phases of chromium alloys, the elastic intensities measured at satellites with nesting vectors parallel and nearly perpendicular to $\boldsymbol{\kappa}$, i.e., at the $(1\pm\delta,0,0)$ and $(\pm\delta,1,0)$ reflections shown in Fig. 2(c), can be used together to determine the polarization of the magnetic state. Neglecting variations in the magnetic form factor due to slightly different momentum transfers, the expected ratios of the elastic satellite intensities for the transversely and longitudinally polarized phases are

$$I_{(1\pm\delta,0,0)}/I_{(\pm\delta,1,0)} = \begin{cases} 2 & \text{TSDW} , \\ 0, & \text{LSDW} . \end{cases} \quad (1)$$

These ratios are independent of magnetic domain structure as the incommensurate scattering at a given satellite is readily identified with a particular nesting vector, that is, a given Q domain. Experimentally, accurate quantitative comparison of intensities is limited as measurements of different magnetic satellites sharing the same domain require changing the orientation of the sample with respect to the incident and scattered beams. Nonideal sample geometry, variations in sample mosaic, extinction, and macroscopic Mn inhomogeneities can each affect observed intensities.

The temperature dependence of the magnetic scattering from CrMn#1 was studied via longitudinal scans along $(h00)$ and $(0k0)$ and transverse scans along $(h10)$ and $(1k0)$. As discussed above, an attempt was made to field cool the sample through T_N, to produce a single-Q$\|$[100] commensurate SDW (CSDW) phase, a day before the neutron-scattering measurements commenced. After removing the field in the CSDW phase, the sample was cooled below $T_{\rm IC}$ to check the resulting domain structure. Comparable scattering intensities were found at the two magnetic domains accessible in the $(hk0)$ scattering plane, Fig. 2(c), indicating that a single-Q sample cannot be produced by field cooling through T_N to the commensurate phase in a 14-T field or that such a commensurate single-Q state relaxes when the field is removed. Additional efforts to field cool the sample through the IC transition, with a 6-T field normal to the scattering plane, also failed to yield any Q-domain imbalance.

In Fig. 3 we show the results of longitudinal (L) scans along $\mathbf{Q}=(0k0)$ and transverse (T) scans along $\mathbf{Q}=(1k0)$ at $T=220$, 140, and 38 K. The data at 220 K are representative of our scattering results in the commensurate phase at temperatures well below T_N. The widths of both spectra reflect the spectrometer resolution and, in the transverse scan, the mosaic of the crystal. The rough equality of the intensities observed in the L and T scans results from the polydomain structure of the sample. At 140 K, the ~2:1 ratio of the L and T satellite intensities is consistent with the TSDW phase polarization dependence presented in Eq. (1) above. The remaining commensurate scattering at this temperature is an artifact of the large vertical acceptance of the spectrometer and scattering arising from the $(0,k,\pm\delta)$ and $(1,0,\pm\delta)$ satellites above and below the scattering plane. At 38 K the polarization of the SDW lies parallel to the nesting vec-

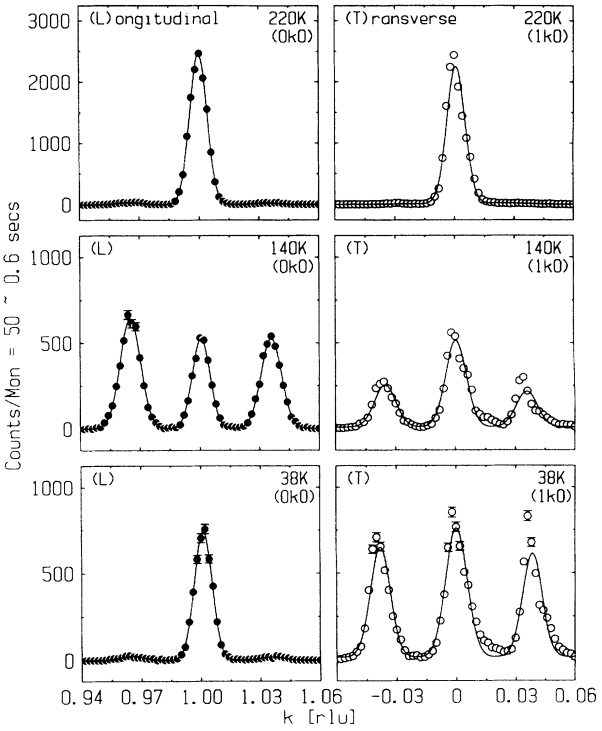

FIG. 3. Longitudinal and transverse data in the commensurate spin-density-wave (SDW) (220 K), transversely polarized incommensurate SDW (140 K), and longitudinally polarized incommensurate SDW (38 K) phases. The commensurate intensity in the incommensurate phases is primarily due to scattering from the $(0,1,\pm\delta)$ and $(1,0,\pm\delta)$ satellites and the large vertical acceptance of the spectrometer. A small fraction of this scattering is also due to commensurate, Mn-rich impurities in the sample.

tors and essentially no satellite scattering is observed in the longitudinal scan. In contrast, the longitudinally polarized moments fully contribute to the satellite intensity in the transverse data. Again, the commensurate intensity in these scans can be attributed to scattering from the satellites above and below the scattering plane. The residual incommensurate intensity visible in the longitudinal data indicates that a small, Mn-rich, portion of the crystal remains in the TSDW phase at this temperature.

The temperature dependences of the commensurate and incommensurate integrated intensities resulting from Gaussian fits to the $(0,h,0)$ (L) and $(1,h,0)$ (T) scans are plotted in Fig. 4. The high-temperature data in the top panel of the figure (★s) are from experiments performed on CrMn#1 at MURR. These data indicate that the majority of CrMn#1 undergoes a paramagnetic to a CSDW transition at $T_N = 455$ K. Some additional scattering, due to Mn-rich portions of the sample, remains present at temperatures above T_N. This scattering decreases with increasing temperature and disappears entirely above 500 K. Below T_N, the commensurate intensities at (1,0,0) and (0,1,0) continue to grow in step. At temperatures below $T \sim 310$ K, scattering is also visible in the incommensurate transverse data at $(1,\delta,0)$ (lower panel). This scattering can be ascribed to Mn-poor ($x \lesssim 0.3\%$) regions in the sample. The intensity resulting from these regions represents 11% of the maximum intensity observed at this satellite. The absence of similar scattering at other satellite positions is due to a misalignment of these regions with the bulk of the crystal.

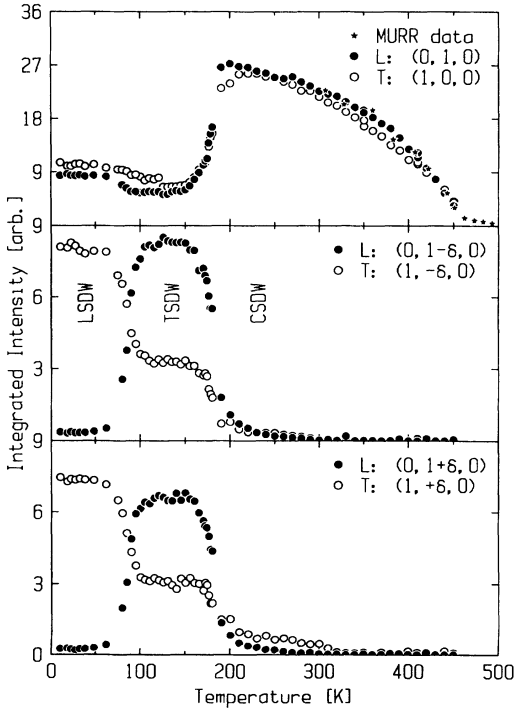

FIG. 4. Integrated intensities at the commensurate and incommensurate positions. The ratios of the longitudinal (○) and transverse (●) intensities at the satellite positions reflect the polarizations of the incommensurate phases.

The magnetic scattering at the incommensurate satellite positions develops abruptly below the IC phase transition. Again, the ratio of the longitudinal (●) and transverse (○) scattering intensities measured in this phase is in rough agreement with the TSDW polarization dependence presented in Eq. (1). The finite intensities visible at the commensurate positions (1,0,0) and (0,1,0) result from the out-of-plane satellites. As reported by Geerken *et al.*,[6] the IC transition in small, homogeneous $Cr_{1-x}Mn_x$ crystals with Mn concentrations of $x = 0.45\%$ and 0.70% is first order and hysteretic. In Fig. 5 we show the evolution of the $(0,1-\delta,0)$ satellite intensity on cooling and heating the sample, over a 12-h period, through the IC transition. Though the distribution of Mn concentrations results in a broad transition, a large fraction of the sample clearly shows a sharp transition on cooling at $T_{IC} = 182$ K. The hysteresis associated with this transition, $\Delta T \sim 20$ K, is also consistent with the behavior observed by Geerken *et al.* and several other authors.[2]

CrMn#1 evinces a spin-flip transition at $T_{SF} = 85$ K. The longitudinal polarization of this low-temperature phase is clearly demonstrated in the approximate doubling, relative to the TSDW phase, of the transverse scan intensity and absence of scattering in the longitudinal data. The residual scattering evident at $(0,1\pm\delta,0)$ again results from the Mn-rich regions of the sample that remain transversely polarized at low temperatures. The intensity of this scattering indicates that these regions constitute ~5% of the total sample volume.

The temperature dependence of the incommensurate wave vector $\mathbf{Q}_- = (1-\delta,0,0)$ is presented in Fig. 6. For

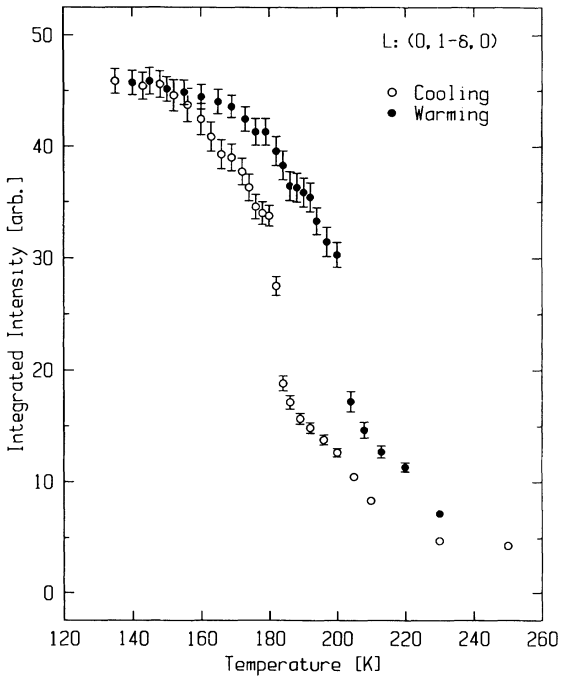

FIG. 5. Twelve-hour hysteresis loop of the $(0,1-\delta,0)$ integrated intensity at the commensurate-incommensurate transition.

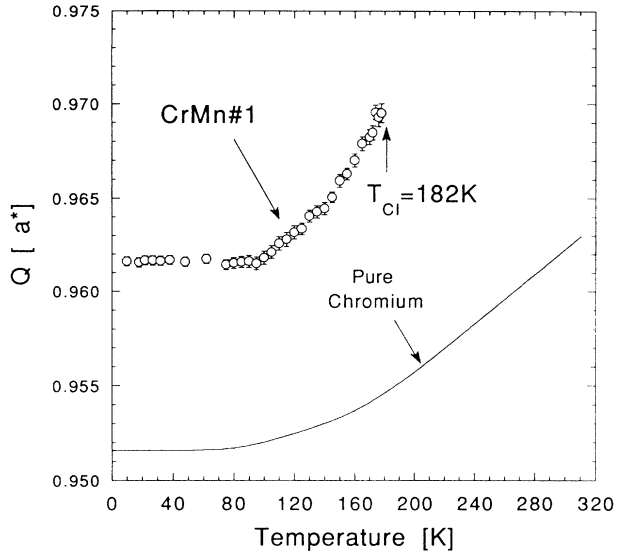

FIG. 6. Temperature dependence of $\mathbf{Q}_{-}=(1-\delta,0,0)$ in CrMn#1 and pure Cr (Ref. 13).

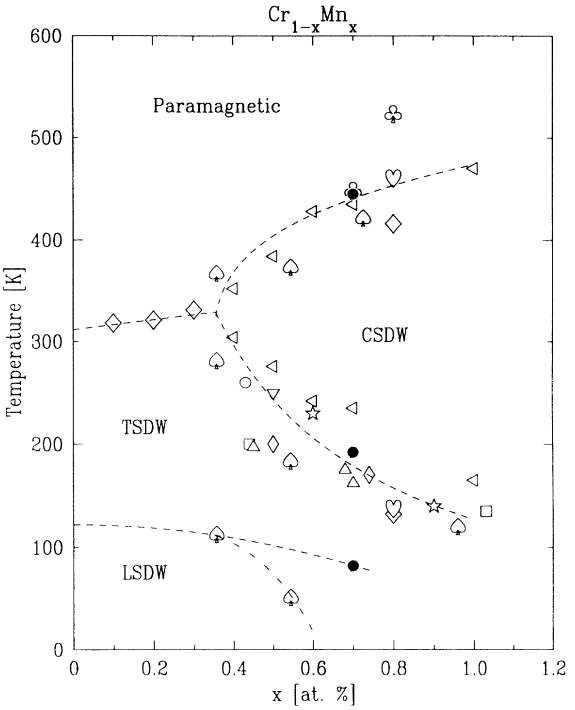

FIG. 7. Phase diagram of $Cr_{1-x}Mn_x$. Transition temperatures from Fig. 4: (●), and additional data from the literature: ♤ (Ref. 5), △ (Ref. 6), ◁ (Ref. 15), □ (Ref. 16), ♣ (Ref. 17), ♡ (Ref. 18), ○ (Ref. 19), and ◇ (Ref. 20).

comparison, the temperature dependence of $\mathbf{Q}_{-}$ in pure chromium, measured by Werner, Arrott, and Kendrick,[13] is also shown. In CrMn#1, the base temperature value of δ, $\delta(0)=0.0383(3)$, remains constant up to $T\approx 105$ K. δ then decreases with increasing temperature to reach a value of $\delta=0.0305(3)$ just below T_{IC}. Similar behavior was observed by Fawcett, Griessen, and Vettier,[14] who attributed the sharp break in the slope of the $\delta(T)$ curve at $T\approx 150$ K in their $Cr_{1-x}Mn_x$ ($x=0.005$) sample to pinning of the SDW by impurity atoms at lower temperatures.

The transition temperatures separating the magnetic phases observed in CrMn#1, $T_N=455$ K, $T_{IC}=182$ K, and in particular, the occurrence of a spin-flip transition at $T_{SF}=85$ K, indicate that the $Cr_{1-x}Mn_x$ phase diagram published in the review of Fawcett, Griessen, and Vettier requires modification. A revised diagram of the temperature and doping dependence of the magnetic properties of $Cr_{1-x}Mn_x$, constructed with the results of our measurements and additional data from the literature, is presented in Fig. 7. As is evident from the figure, our values for T_N and T_{IC} are consistent with earlier $Cr_{1-x}Mn_x$ work. However, the spin-flip transition temperature we observe is sharply at odds with the earlier work at Koehler *et al.*[5] The comparatively high spin-flip temperature extracted from the data of Fig. 4 demonstrates that the spin-flip transition is much more weakly dependent on electron doping than previously thought. Measurements to study the relationship between T_N, T_{IC}, and T_{SF} at higher Mn concentrations are currently underway.

ACKNOWLEDGMENTS

We wish to thank Dr. Lawrence G. Rubin of the Francis Bitter National Magnet Laboratory for his help and advice during our efforts to single-Q CrMn#1. Invaluable technical assistance was provided by R. Rothe, J. Biancarosa, and R. J. Liegel. Work at Brookhaven National Laboratory was carried out under Contract No. DE-AC0276CH00016, Division of Materials Science, U.S. Department of Energy. S.A.W. would like to acknowledge the support of the NSF through Grant No. NSF-PHY 9024608 and E.F. the Natural Sciences and Engineering Research Council of Canada.

[1]E. Fawcett, Rev. Mod. Phys. **60**, 209 (1988).
[2]E. Fawcett *et al.*, Rev. Mod. Phys. **66**, 25 (1994).
[3]A. Arrott, S. A. Werner, and H. Kendrick, Phys. Rev. Lett. **14**, 1022 (1965).
[4]J. P. Hill, G. Helgesen, D. Gibbs, and G. Shirane (private communication). Recent time-dependent measurements suggest that the order of the antiferromagnetic transition at T_N in chromium requires additional study.
[5]W. C. Koehler, R. M. Moon, A. L. Trego, and A. R. Mackintosh, Phys. Rev. **151**, 151 (1966).
[6]B. M. Geerken *et al.*, J. Phys. F **12**, 1603 (1982).
[7]S. K. Burke, W. G. Stirling, K. R. A. Ziebeck, and J. G. Booth, Phys. Rev. Lett. **51**, 494 (1983).
[8]E. Lorenzo, B. J. Sternlieb, G. Shirane, and S. A. Werner,

Phys. Rev. Lett. **72**, 1762 (1994).
[9]D. R. Noakes, T. M. Holden, E. Fawcett, and P. C. de Camargo, Phys. Rev. Lett. **65**, 369 (1990).
[10]To achieve measurable scattering intensities, triple-axis spectrometers are generally designed with coarse momentum resolution normal to the scattering plane.
[11]P. C. de Camargo, E. Fawcett, and J. M. Perez, J. Appl. Phys. **67**, 5265 (1990).
[12]G. L. Squires, *Introduction to the Theory of Thermal Neutron Scattering* (Cambridge University Press, Cambridge, England, 1978).
[13]S. A. Werner, A. Arrott, and H. Kendrick, Phys. Rev. **155**, 528 (1967).
[14]E. Fawcett, R. Griessen, and C. Vettier, in *Transition Metals, 1977,* Proceedings of the International Conference on Transition Metals, IOP Conf. Proc. No. 39, edited by M. J. G. Lee, J. M. Perez, and E. Fawcett (Institute of Physics and Physical Society, London, 1978), p. 592.
[15]A. K. Butylenko and V. V. Nevdacha, Ukr. Fiz. Zh. (Ukr. Ed.) **25**, 137 (1980).
[16]T. J. Bastow, Phys. Rev. B **88**, 935 (1966).
[17]A. Jayaraman, T. M. Rice, and E. Bucher, J. Appl. Phys. **41**, 869 (1970).
[18]P. R. Peretto, R. Venegas, and G. N. Rao, Phys. Rev. B**23**, 6544 (1981).
[19]Y. Syono and Y. Ishikawa, Phys. Rev. Lett. **19**, 747 (1967).
[20]J.V. Yakhmi, I. K. Gopalakrishnan, and R. M. Iyer, J. Phys. F **14**, 923 (1984).

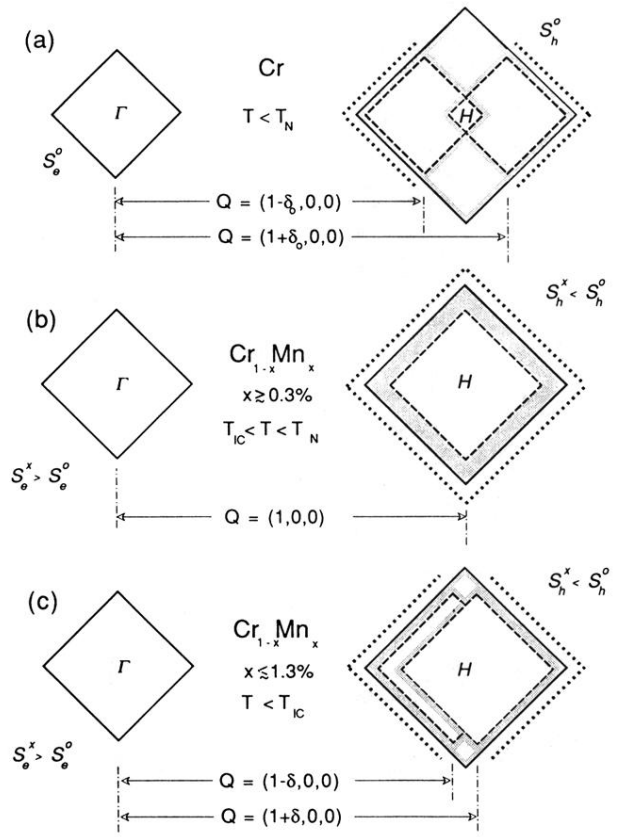

FIG. 1. Nesting of electron Γ and hole H Fermi surface octahedra in (a) pure Cr and (b), (c) $Cr_{1-x}Mn_x$. The dissimilar size of these two surfaces in pure Cr results in nesting that is incommensurate at all temperatures below T_N. In $Cr_{1-x}Mn_x$, for $x \gtrsim 0.3\%$, the nesting vector, and consequently the resulting spin-density-wave phase, are commensurate (b) with the crystal lattice below the Néel transition T_N. At lower temperatures, provided $x \lesssim 1.3\%$, the free energy of $Cr_{1-x}Mn_x$ favors a transition to incommensurate nesting (c).

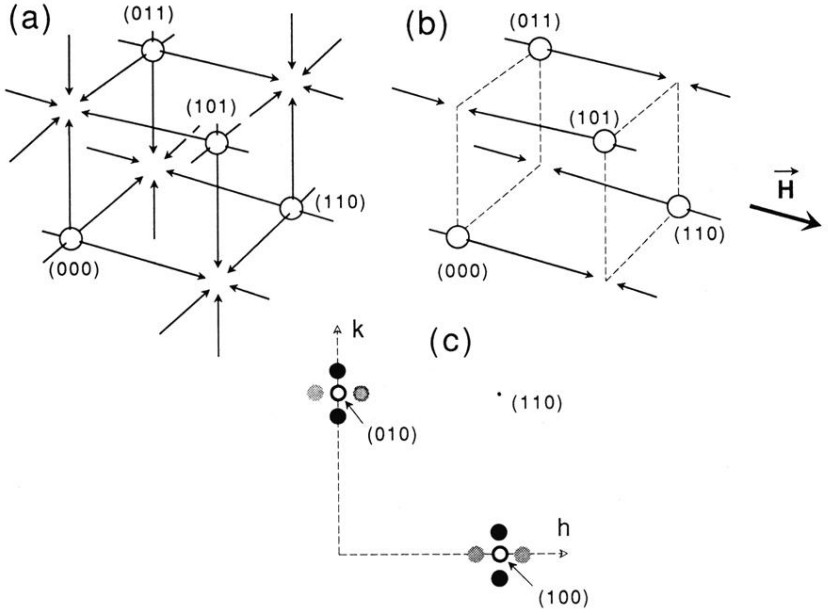

FIG. 2. Reciprocal space showing magnetic (arrow heads) and nuclear (circles) Bragg reflections in (a) polydomain- and (b) single-**Q** Cr. The gray and black circles shown in the $(hk0)$ scattering plane (c) indicate the two distinct **Q** domains in an incommensurate, polydomain sample accessible in this scattering geometry. Finite spectrometer resolutions allow the satellites above and below the plane to contribute to the observed scattering intensity at the commensurate positions (open circles).